SAND2019-14592C

Burst-Mode Spontaneous Raman Thermometry in a Flat Flame

Caroline Winters[1], Sean Kearney[2], and Justin Wagner[3]
Sandia National Laboratories, Albuquerque, NM 87123, USA

Timothy Haller[4] and Philip Varghese[5]
Department of Aerospace Engineering and Engineering Mechanics
The University of Texas at Austin, Austin, TX 78712-1221

A high-speed Raman thermometry diagnostic was evaluated in lean H_2-air flames at a data acquisition rate of 5 kHz. Bursts of nanosecond pulses were generated at a 10 kHz burst rate with energy of E ≈ 13 J/burst at λ = 532 nm. The pulses had duration of order 200 ns and were used to interrogate a stabilized flat flame burner. Spectra were collected using a spectrometer having focal length 0.32 meters and an electron multiplying charge-coupling device (EMCCD) detector. Raman spectra were integrated over the full burst to map adiabatic flame temperature versus equivalence ratio. The measured spectra resolved vibrational band features to infer temperature. A detailed spectral fitting model was used in the burst-integrated and burst-mode spectra. Two pulses were used for each burst-mode measurement resulting in a 5 kHz rate up to flame temperatures of about 2100 K. The measurement precision in burst mode was 23 K and 62 K at flame temperatures of 1160 K and 2080 K, respectively. The measurement accuracy was benchmarked against the spectrally fitted full-burst spectra, chemical equilibrium calculations and previous coherent anti-Stokes Raman (CARS) measurements. Finally, a path towards demonstration of this technique in a high-temperature shock tube is briefly outlined.

I. Introduction

Measurements in high-speed, high-enthalpy flows necessitate high-repetition diagnostics. This is particularly true in impulsive facilities such as shock tubes and shock tunnels where experimental times are often on the order of one millisecond (ms) or less. An ideal diagnostic in impulsive facilities should: 1) generate sufficient signal at extreme

---

[1] Senior Member of the Technical Staff, Fire Sciences, P.O. Box 5800, Mailstop 0828; cwinte@sandia.gov AIAA Member.
[2] Distinguished Member of the Technical Staff, Engineering Sciences Center, AIAA Associate Fellow
[3] Principal Member of the Technical Staff, Engineering Sciences Center, AIAA Senior Member.
[4] Graduate Student, AIAA Member
[5] Distinguished Teaching Professor, 1 University Station, C0600 Austin, TX, AIAA Associate Fellow

Sandia National Laboratories is a multi-mission laboratory managed and operated by National Technology and Engineering Solutions of Sandia, LLC., a wholly owned subsidiary of Honeywell International, Inc., for the U.S. Department of Energy's National Nuclear Security Administration under contract DE-NA0003525.

pressure and temperature, 2) acquire data at rates faster than post-shock event lifetimes and 3) provide spatial and temporal resolution within the tube.

Techniques like optical emission spectroscopy (OES), laser absorption spectroscopy (LAS) and laser induced fluorescence (LIF) are routinely used in shock tubes for temperature inference due to their robustness and design simplicity; however, OES and LAS suffer from a lack of spatial resolution [1,2,3]. OSES additionally relies on upper state transition emissions, which may not reflect the larger ground state population [4]. LIF requires fluorescence quenching calibration adding additional uncertainties. Moreover, at high pressures, the quenching cannot be resolved by nanosecond pulsed, high repetition rate lasers [5].

Inferring temperature from spectrally resolved light scattered off a measurement species is another approach to laser-based thermometry. Scattering techniques include Rayleigh scattering, Raman spectroscopy, and CARS. Over the years, there has been significant effort to advance and improve light-scattering thermometry to ever more challenging optical environments [6,7,8,9,10]. Rayleigh scattering produces a strong signal but requires knowledge of the gas composition at every measurement point and can be easily overwhelmed by scattering interference from the incident laser beam. A CARS signal beam is spatially and frequency discrete but requires multiple beams to be overlapped in space and time. This can be particularly challenging in the dynamic environment of a shock tube. Spontaneous Raman spectroscopy offers the robustness of a single probe-detector configuration, while providing discrete signal spatially and temporally. It has been previously demonstrated in luminous, rich hydrocarbon flames and turbulent jets [11,12].

Addressing the outlined criteria for testing in a shock tube, Raman signal to noise can be increased by adjusting the spectral resolution of the measurement, in effect spectrally integrating along the vibrational bands. Temperature inference from vibrational band populations has been well-validated and is employed in this work [9,13]. Multiple measurements over a millisecond test time requires data rates greater than a kilohertz. Previous work suggests interrogation by a high-speed "burst" of laser pulses can offer high-speed measurements. Additionally, pulse-bursts have megahertz (MHz) repetition rates, allowing integration of multiple laser pulses for kilohertz sensing, which will mitigate effects of low signal-to-noise ratio (SNR).

Previous work has demonstrated high-speed Raman imaging in flames at 10 kHz to study relative species concentrations and qualitative temperatures [14,15,16]. Additionally, high-speed relative species concentrations were made in a near-adiabatic flat flame using integrated Raman signal; the temperature measurements, however, were made using Rayleigh scattering [17]. Raman thermometry requires spectrally resolved measurements and has thus far been limited by the laser repetition rate. Temperatures in shear boundary layers have been made using a 10 Hz Nd:YAG laser, with significant time integration [18]. Furthermore, well-resolved Raman signals have provided information about the state of equilibrium of a supersonic flow, identifying regions of non-equilibrium, by comparing rotational and vibrational energy distributions [18]. Finally, Raman spectroscopy can achieve spatial resolution on the order of millimeters and temporal resolution on the order of nanoseconds depending on the required laser pulse duration to avoid breakdown.

The present work leverages a pulse-burst laser to develop a new diagnostic capable of spatially resolved, accurate measurements at speeds faster than state-of-the-art laser-based thermometry. These measurements are demonstrated at 5 kHz in a H_2-air Hencken burner over equivalence ratios of 0.29 – 0.73, which corresponds to flame temperatures, *T,* ranging from 1160 K – 2080 K. Signal collected in side-scatter (90° with respect to the probe volume) was compressed onto an EMCCD detector using a $f/4.1$ spectrometer, in conjunction with a set of relay lenses. This detector has been used previously to collect spectra at 100 kHz by illuminating 10 chip rows every shot [7]. Here, pulse-burst Raman spectroscopy is determined to be an accurate and precise technique for temperature measurements. A brief discussion of the anticipated challenges in applying this diagnostic in high-enthalpy shock tube flows follows.

II. Experimental Design

A. Spontaneous Raman Spectroscopy

Raman is a form of vibrational/rotational spectroscopy performed on homonuclear molecules, like N_2 or O_2. The method resolves the inelastically scattered, Stokes-shifted photons, which are red-shifted in frequency with respect to the incident light. The magnitude of frequency shift corresponds to the molecular species of interest and its internal energy. When a molecule is in thermal equilibrium, an increase in translational energy also results in an increase in vibrational energy. The hotter the molecule, the more vibrational energy levels will be populated and the lesser the population occupying the ground state.

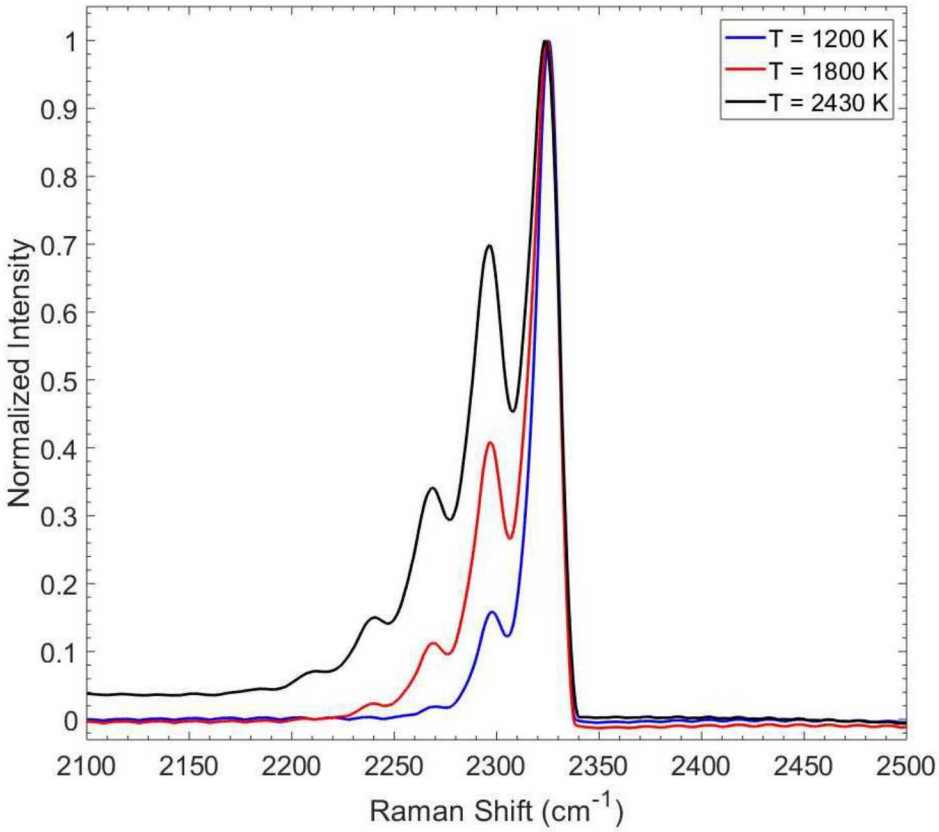

Figure 1: Normalized simulated nitrogen Raman spectra demonstrating temperature dependent vibrational level population. The temperatures correspond to those probed using the burst-mode thermometry.

Examples of simulated Raman spectra over the present experimental measurement range are shown in Fig. 1. The majority of the simulated nitrogen population lies in the first vibrational state at the lowest temperature of T = 1200 K. The second and third vibrational states have been populated by 1800 K. A significant population has shifted to the second vibrational level by 2250 K. This depopulation of the ground state must be a consideration when applying Raman spectroscopy to extreme temperature environments. Additionally, the Raman signal, S_{Raman}, is weak and is linearly dependent on the environment according to:

$$S_{Raman} = Pnf\frac{\partial\sigma}{\partial\Omega}\varepsilon l\Omega \qquad \text{(Eqn. 1)}$$

where P is the incident laser power, n is the target species number density, $\frac{\partial\sigma}{\partial\Omega}$ is the Raman cross-section of the molecular species, ε is the detector's efficiency, l is the sampling length set by the probe volume, and Ω is the collection solid angle [18]. An increase in Raman signal can therefore be achieved by increasing either the acquisition integration times, or the laser fluence to the probe volume. The former is acceptable at steady-state conditions but reduces or removes temporal resolution. The latter can result in perturbation of the measurement volume, by laser-induced heating, or negation of the measurement due to laser-induced breakdown. Accurate measurements have been readily obtained by stretching a laser pulse to hundreds of nanoseconds, allowing hundreds of millijoules of laser energy into the system [19,20,21].

B. Pulse-burst laser and burner

A multi-stage, diode and flashlamp pumped Spectral Energies Quasimodo pulse-burst laser was used for flame interrogation. The laser operated at 10 kHz over a total burst duration of 2.5 ms. For this study, the laser was modified to accept a Thorlabs continuous wave (cw) diode seed laser (model DBR1064P) at $\lambda = 1064$ nm. An arbitrary wave generator (AWG) was programed to shape the seed into Gaussian laser pulses approximately 200 ns in duration. These pulses were then amplified and doubled to produce an energy of ≈13 J per burst (≈ 0.52 J per pulse). The laser energy was monitored daily with an Ophir VEGA power meter. The burst energy was maximized by tuning the seed-diode temperature to allow optimal conversion efficiency for $\lambda = 532$ nm light generation.

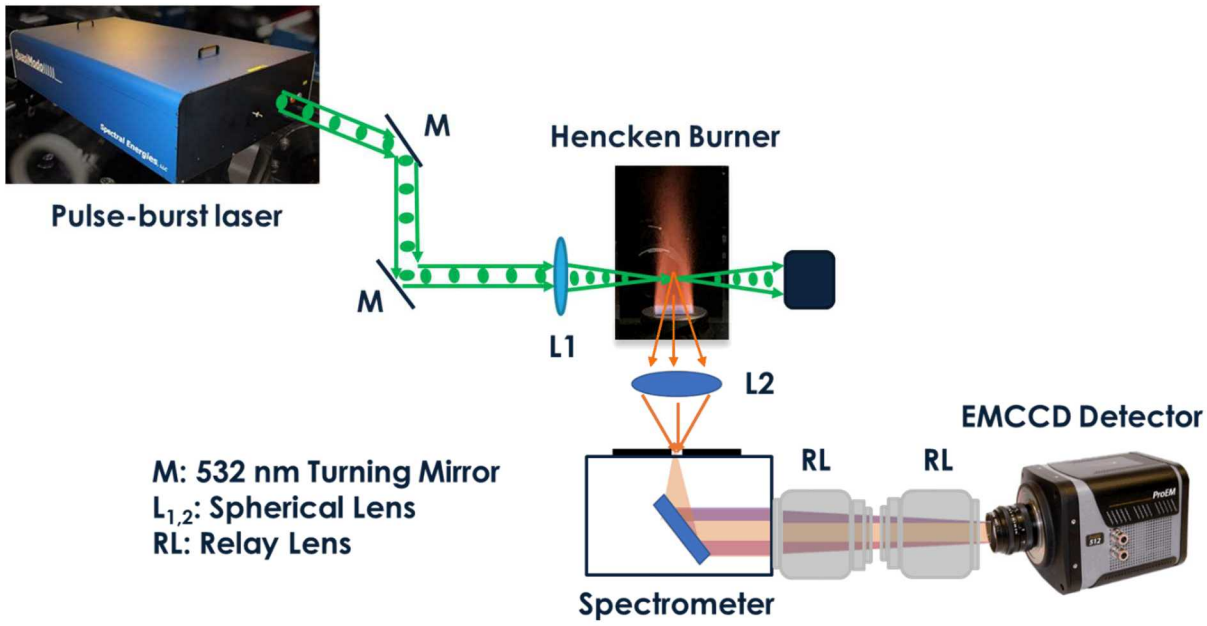

Figure 2: Experimental schematic to collect burst-mode Raman spectroscopy in a flame.

The experimental design is given in Fig. 2. The laser burst was focused to a height of 12.7 mm above the center of a stabilized flat flame burner (details to follow) using a spherical lens having a focal length $f = 500$ mm. The scattered light was collected and collimated at 90° from the incident axis of propagation by an achromat lens having a 100 mm focal length (f/2). The collimated light then passed through a periscope to account for the height difference between the burner and the spectrometer. Care was taken to account for the polarization of the Raman signal. The signal was imaged onto the spectrometer slit, opened to 200 micrometers (um), by a spherical lens with a 200 mm focal length (f/4). The spectrometer, a Horiba Jobin Yvon iHR320 having a focal length of 0.32 meters (f /4.1), was aligned using the Rayleigh scattering from the probe volume. The light was dispersed onto the detector by a 1200 groove/mm grating blazed at 500 nm. The grating efficiency was approximately 50% at the Raman shift wavelength.

A wavelength calibration and alignment check was performed using an Oriel 6032 neon pen lamp. A pen lamp spectrum and corresponding calibration curve is shown in Figure 3.

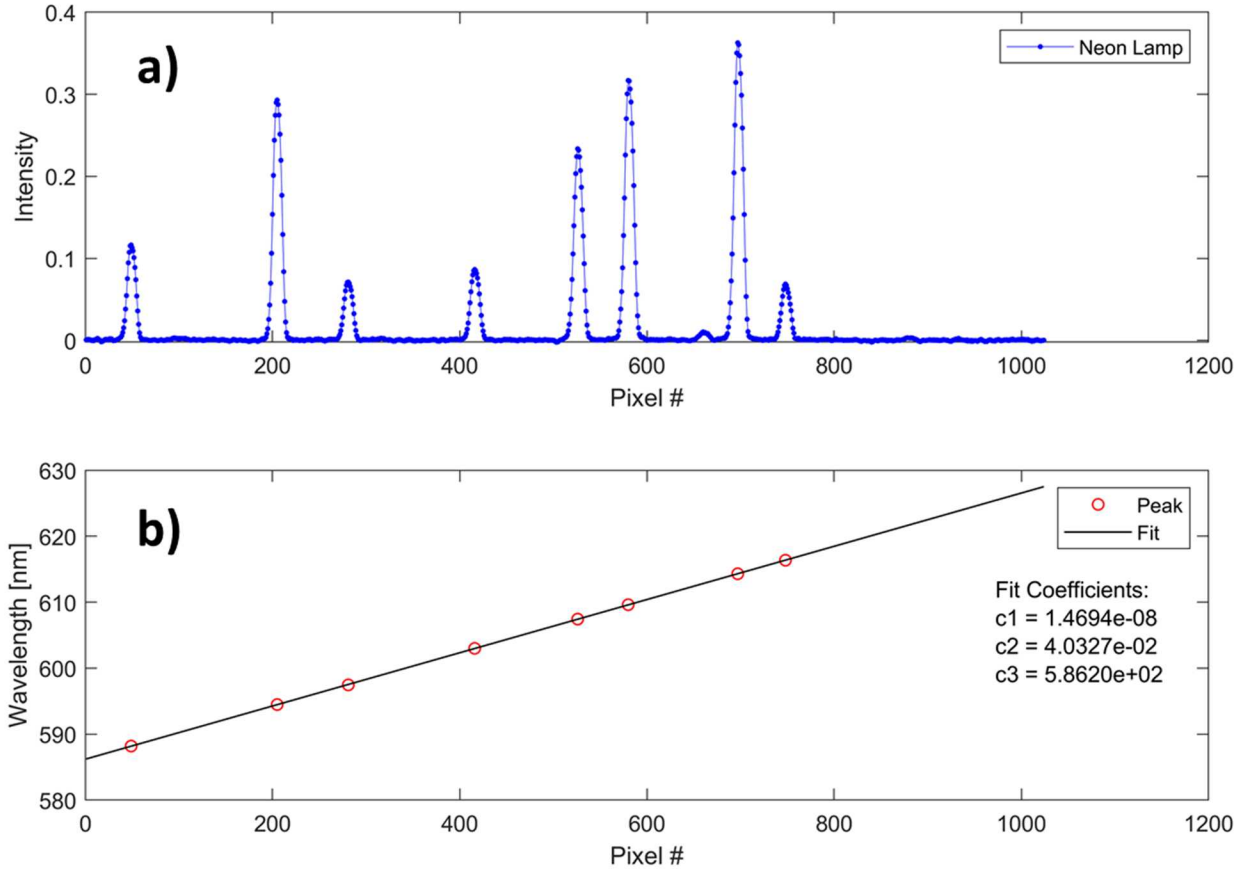

Figure 3: a) Neon lamp spectra and b) resulting wavelength calibration for the spectrometer and detector system.

The relative positions and intensities of the neon pen lamp spectra were compared to the NIST database to identify five emission transitions [22]. The line positions were then correlated with the pixel number to generate a wavelength calibration for the Raman spectra. Additionally, the atomic emission transitions from the pen lamp are taken to be nearly Dirac delta function, such that any spectral line broadening is the convolution of the atomic transition and experimental instrument function associated with the collected light passing through the micrometer-scale entrance slit.

C. EMCCD Detector

After the light was spectrally dispersed by the spectrometer's grating, it was imaged onto a Princeton Instruments back-illuminated EMCCD detector (Model ProEM-HS:1024BX3). The detector contained a 1024 x 1024-pixel chip with 13 um x 13 um pixel size and had a maximum acquisition rate of 100 kHz. To resolve the Raman signal from the entire 10 kHz burst, the detector was operated in 'Full Frame', 'Low Noise' mode. In this mode, the full chip was exposed for a time of 2.6 ms, which was gated around the 2.5 ms laser pulse-burst. The signal was then binned into a single 1024-pixel row and read from the chip. To collect multiple frames of Raman signal from the laser burst at a 5 kHz data acquisition rate, the detector was operated in 'Kinetics', 'EM Gain mode': In this mode, the bottom 280 rows were illuminated during two exposures (laser pulses) in the burst. These rows were then binned and transferred upwards on the chip to allow for the next 280 rows to be illuminated. This detector architecture allowed a

burst of frames to be taken in accordance with the laser burst. Fig. 3 provides example images of the Raman signal from a single laser pulse in full frame and in burst frame (1024 x 280 pixels) mode operation.

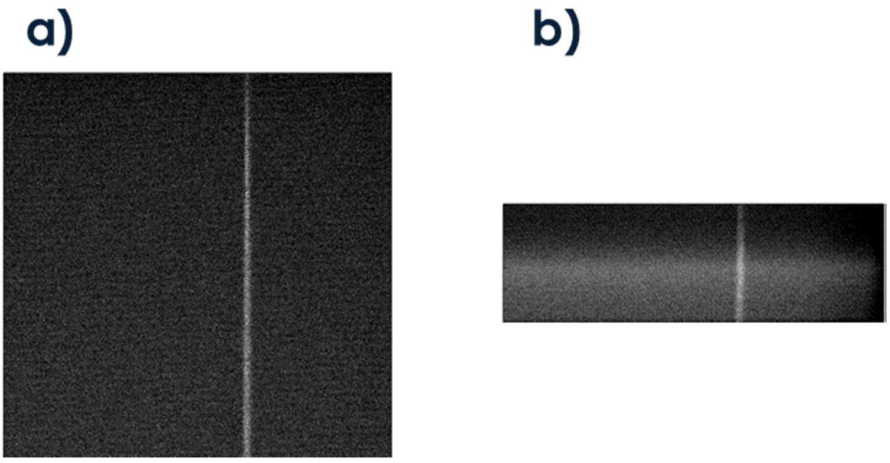

Figure 4: EMCCD camera images of the a) full frame (1024 x 1024 pixels) and b) burst frame (1024 x 284 pixels) Raman signal

In Kinetics mode, the camera chip is always exposed, making light interference mitigation critical for high-speed data collection. A set of Nikon Camera relay lenses with focal lengths of 50 and 101 mm were placed between the exit plane of the spectrometer and the detector chip. This served to prevent extraneous light interference during the chip exposure and to compress the Raman signal. The 280-row limitation for burst-mode operation also required a 3.5 mm mask to be placed in front of the spectrometer slit to prevent inadvertent exposure to the remaining rows. The detector height was then translated to ensure the upper part of the chip was not exposed to any extraneous light. Note that in all cases, the spectra had no background subtraction due to shot-to-shot variance in the baseline and there was minimal interference from luminescence and scattered light

A total of seven frames were taken for every laser-burst. Figure 5 shows the relative camera timing to the laser pulse-burst.

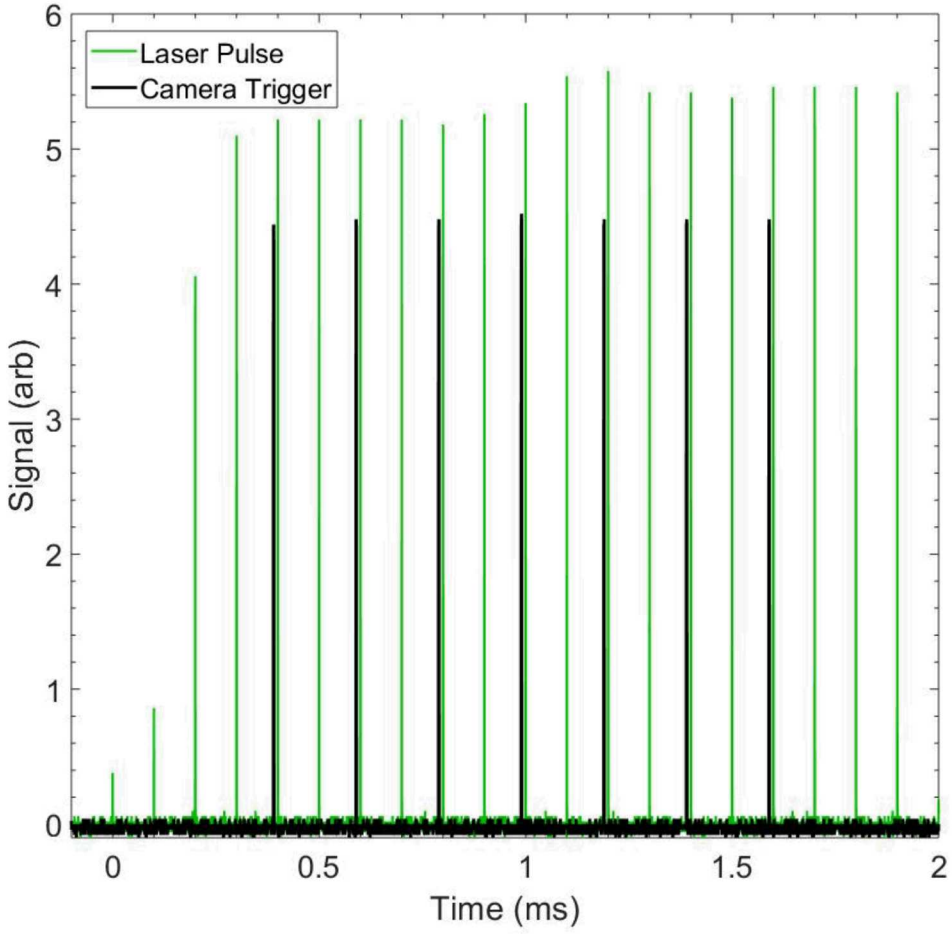

Figure 5: Timing of the camera and laser trigger used to acquire Raman at 5 kHz. The first camera image integrates the first four laser pulses, whereas the remaining six pulses integrate two laser pulses each.

As seen previously, the pulse-burst laser produces weaker laser pulses in the beginning of the burst before the pulse energy stabilizes [23]. The camera triggering began after the fourth laser pulse, within the stable region of the pulse-burst.

D. Stabilized Flat Flame

Finally, the pulse-burst laser was used to interrogate a stabilized flat flame known as a Hencken burner. The Hencken burner is generated by hundreds of small, candle-like flames, set across its area A of 2500 mm^2. The burner shown in Figure 6.

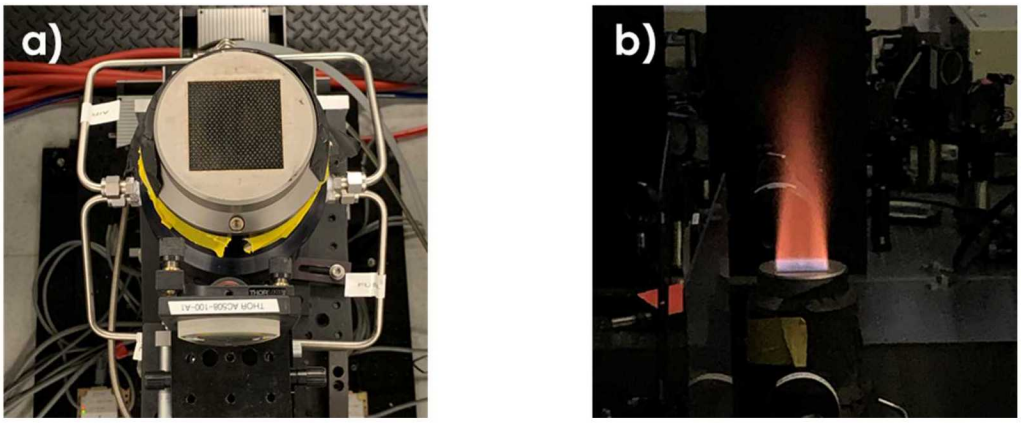

Figure 6: a) Top-down image of the Hencken burner and b) H_2-air flame at $\phi \approx 0.73$.

The equivalence ratio of the flame, and therefore the flame temperature, was varied by mixing a constant volumetric flow rate of air ($\dot{v}$ = 86 SLPM) with hydrogen at varying volumetric flow rates of 8- 24 SLPM. The flow rate was set using MKS 1559a mass flow controllers and MKS 246C controller readouts. The standard accuracy for the hydrogen controller is 2% of the full scale, or 1 SLPM of hydrogen; the standard accuracy for the air controller is 1% FS, or 2 SLPM of air. The precision of the readout is 1% for the air controller. When using a gas correction factor (GCF), which is necessary for hydrogen, this precision is reduced to 5%. The signal on the detector was maximized using room temperature air before measurements were taken in the Hencken burner.

III. Results and Discussion

A. Full-burst Raman Thermometry

Vibrational Raman signal was initially collected over the full 2.5 ms of the laser burst. The stabilized Hencken burner operated at equivalence ratios of ϕ = 0.29 – 1.23. These ratios were anchored to chemical equilibrium calculations of adiabatic flame temperatures [24]. The burst-mode spectra had SNR ≈ 50 – 180 and were used to map flame temperatures to H_2-air equivalence ratio. A spectrum of the Raman signal at ϕ= 1.07 is shown in Figure 7.

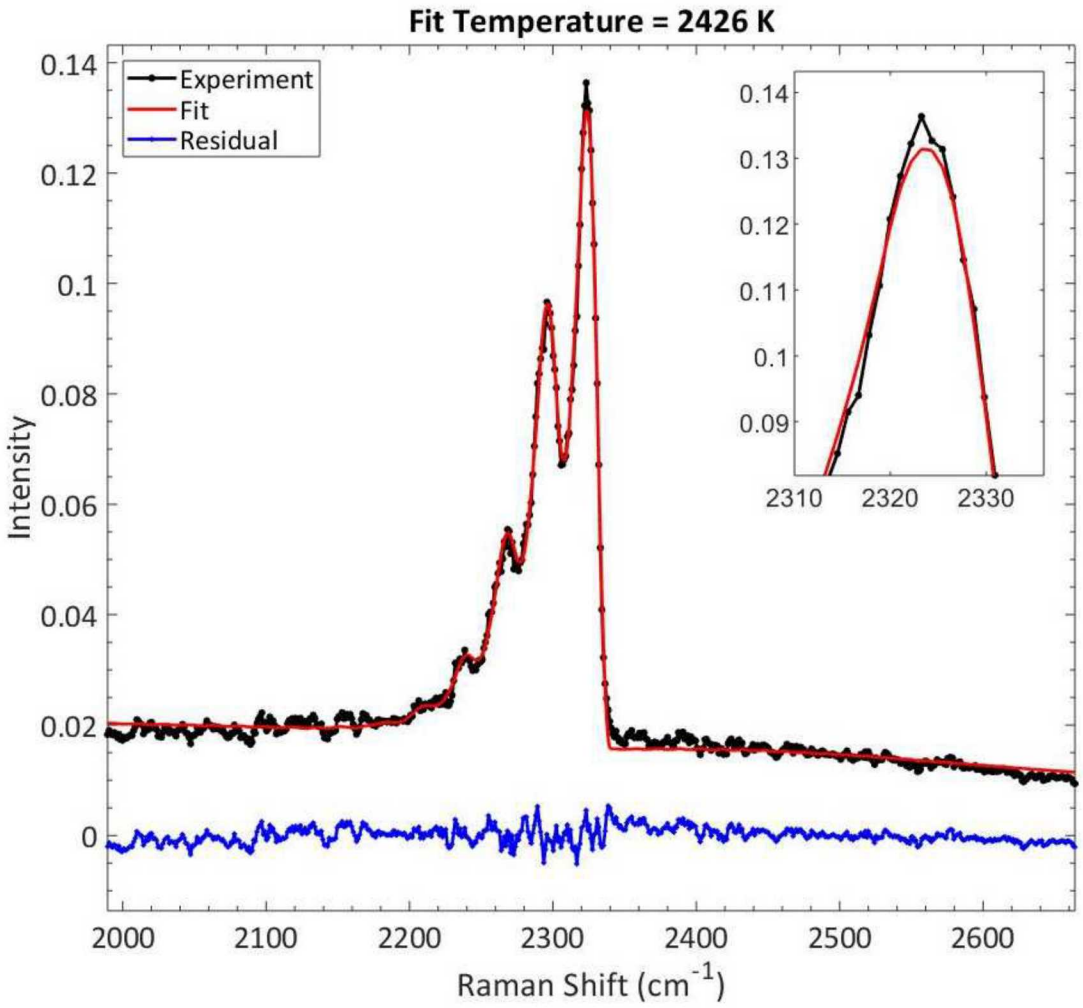

Figure 7: Full-burst Raman spectrum with superposed best fit taken over 2.5 ms in a H_2-air flat flame at ϕ= 1.07.

The resolved spectral peaks in Fig. 7 were all Q-branch Raman transitions. A Fortran spectral physics model was provided by the University of Texas at Austin [13]. Fits were generated using tabulated molecular constants, the measured instrument function and linewidths (Fig. 3a), and the gas mixture. The temperature of the gas was then inferred from the relative intensities of the vibrational bands. The spectrum in Fig. 7 was best-fit to a peak temperature of 2426 K, which is slightly higher than published adiabatic flame temperatures previously made in this burner [7,25]. The standard deviation σ of the full-burst Raman measurement was $\pm$ 23 K determined from five full-burst spectra. Full-burst Raman spectra also provided a measurement of the vibrational band lineshapes. Determination of the lineshapes was necessary for generating meaningful fits of the Raman spectra and was further applied to the burst-mode Raman spectra.

Measured temperatures with precision (standard deviation here) are compared to temperatures from chemical equilibrium calculation in Figure 8.

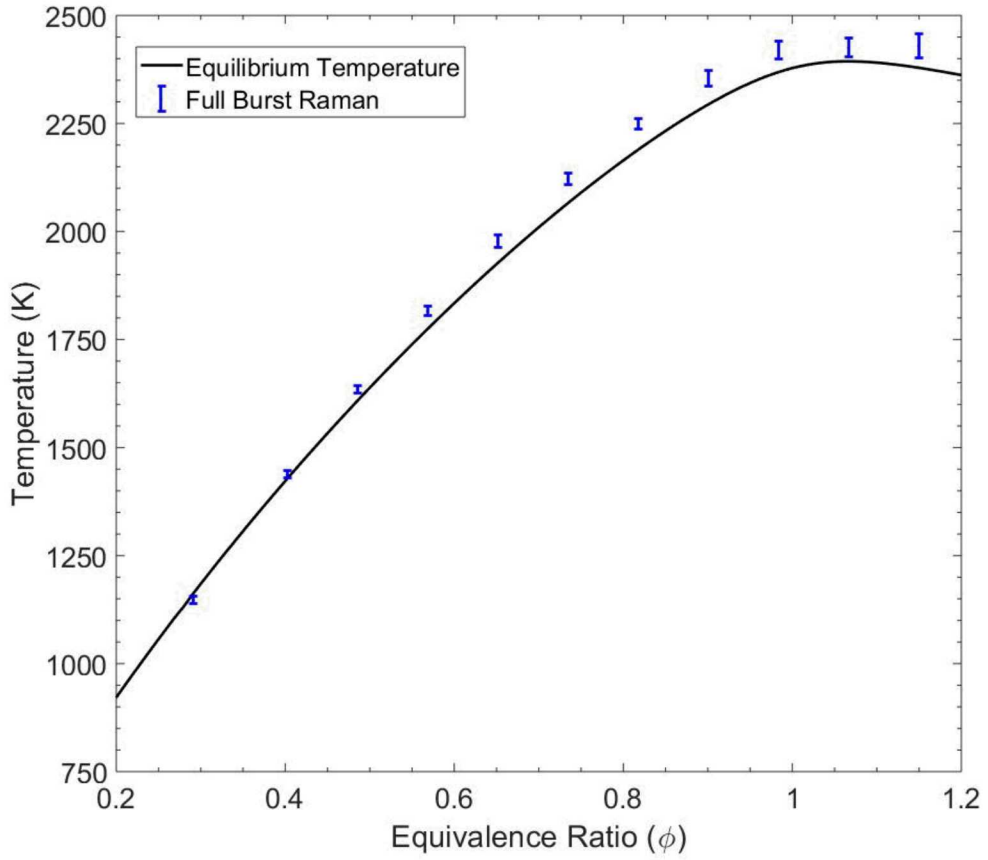

Figure 8: H_2-air gas mixture equivalence ratio versus chemical equilibrium temperatures (black line) and flame temperatures inferred from full-burst integrated Raman spectra (blue symbols) taken over 2.5 ms.

The temperature measurements were systematically higher than calculated flame temperatures for gas mixtures of $\phi > 0.5$. Determination of measurement accuracy of the full-burst Raman thermometry was made by comparing the percent difference between the mean temperature and chemical equilibrium temperature. The maximum percent difference 3.9% at an equivalence ratio of $\phi = 0.73$. At near stoichiometric conditions ($\phi = 0.99$), the accuracy of the measurement was 1.35%.

B. Burst-mode Raman Thermometry at 5 kHz repetition rate

High-speed Raman temperature measurements were made every 200 μs throughout the burst. As previously mentioned, the camera was run at 5 kHz and each frame was exposed to two laser pulses in the 10 kHz burst. Each burst generated a set of spectra an example of which is shown in Figure 9.

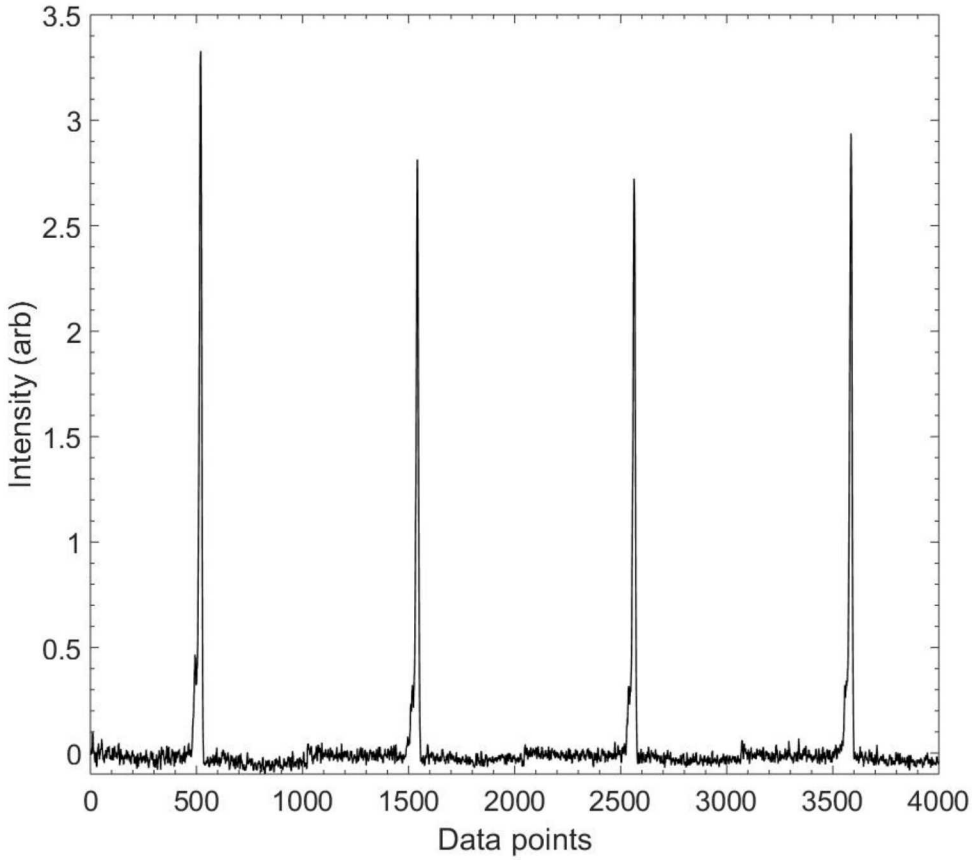

Figure 9: Four raw frames of pulse-burst Raman spectra taken in a H_2-air flame with $\phi = 0.29$ at a 5 kHz data acquisition rate.

For measurement precision and accuracy determination, at least twenty pulse-burst spectra were taken at each equivalence ratios from $\phi = 0.29 – 0.73$ in the stabilized H_2-air flame. A magnified single exposure Raman spectrum from the leanest flame is shown in Figure 10a; Fig. 10b is the same spectrum binned horizontally, with the best-fit for temperature inference shown in Fig. 10c.

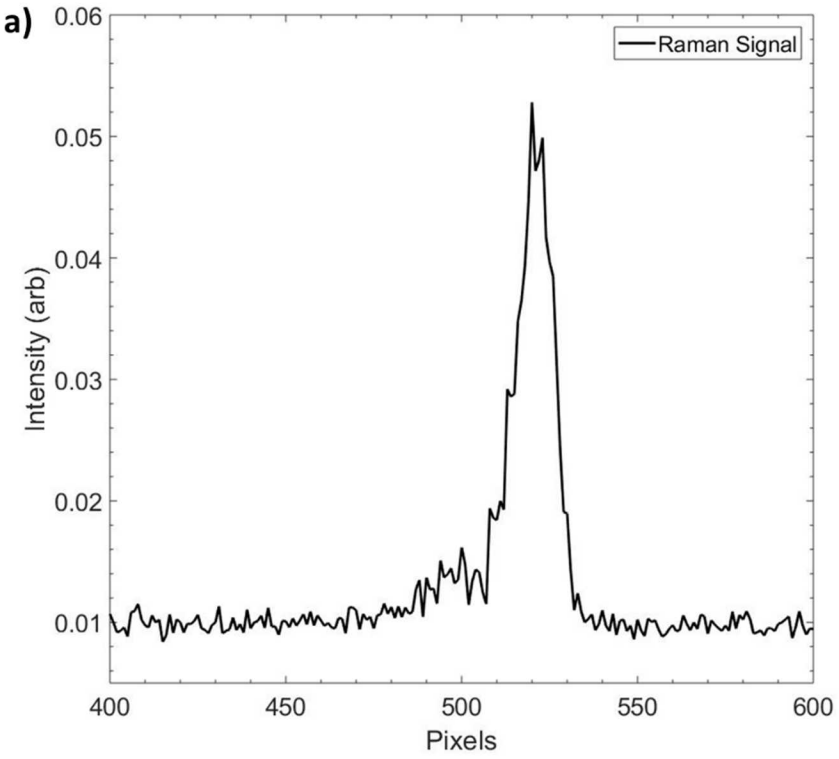
a)
Raman Signal
Intensity (arb)
Pixels
0.06
0.05
0.04
0.03
0.02
0.01
400
450
500
550
600

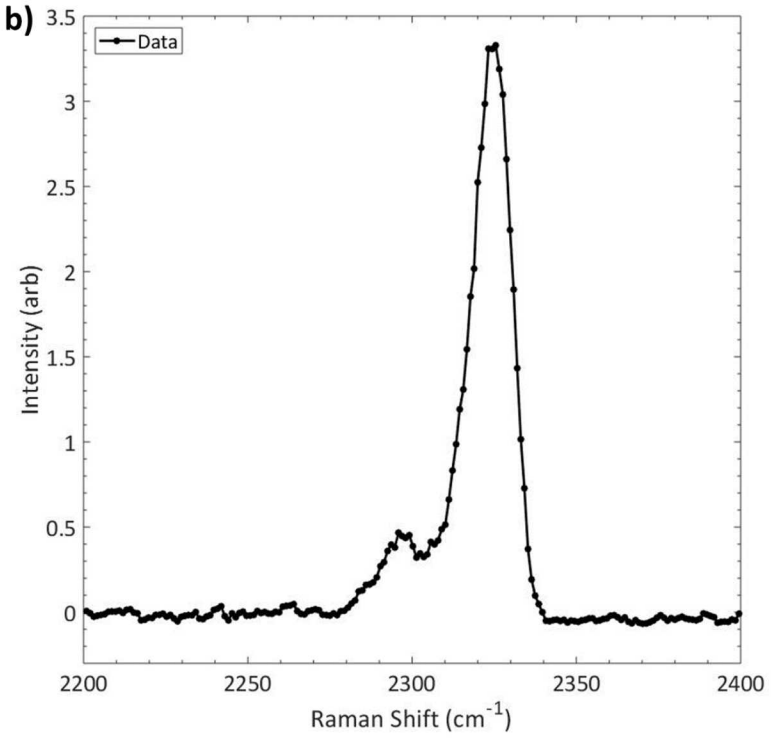
b)
Data
Intensity (arb)
Raman Shift (cm-1)
3.5
3
2.5
2
1.5
1
0.5
0
2200
2250
2300
2350
2400

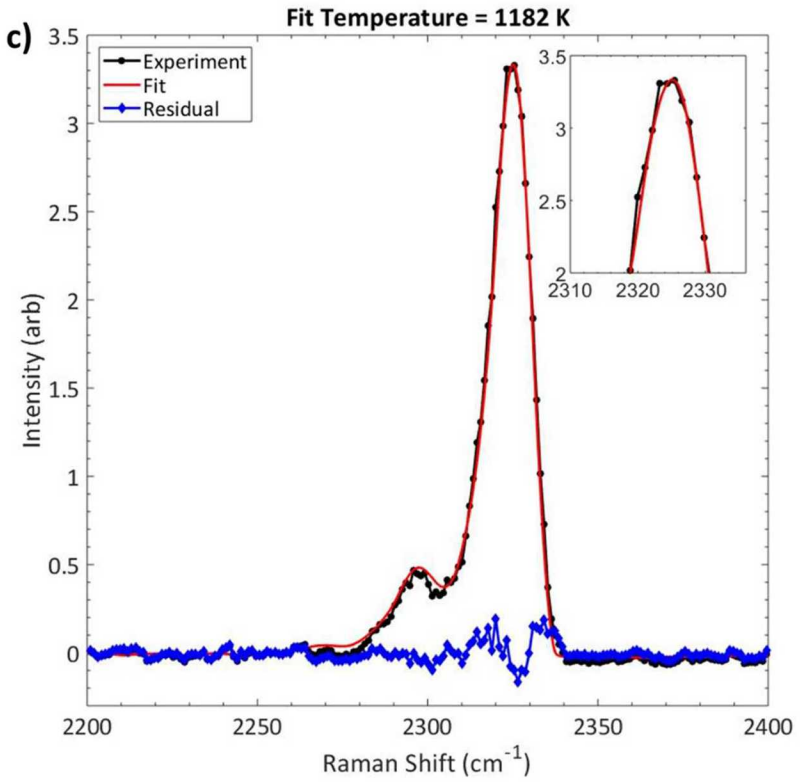

Figure 10: a) Example 5 kHz raw Raman spectrum at a flame temperature of 1182 K and $\phi = 0.29$, b) spectrum binned horizontally by 4 pixels and c) binned spectrum with superposed best fit temperature.

By applying a horizontal bin of four pixels across the chip, the peak signals were improved with minimal impact to spectral resolution. The inferred gas temperature of the flame from Fig. 10c was $T = 1182$ K; the mean flame temperature based on all twenty-one spectra collected at this equivalence ratio was $T_{mean} = 1160 \pm 23$ K. Here and throughout the paper, the precision about the mean is taken to be the standard deviation. At this temperature, most nitrogen molecules occupied the first vibrational state; the peak of the second vibrational state was nearly seven times less than the ground state peak. Each exposure in the pulse-burst was fit independently for temperature, providing the measurement precision of $\pm$ 23 K.

The operation range of the burst-mode Raman thermometry operation was determined by increasing the H_2 mixture fraction until the SNR fell to approximately 5. This corresponds to $\phi = 0.73$ and a flame temperature of about 2080 K. The resulting binned spectrum and superposed best-fit are shown in Figure 11.

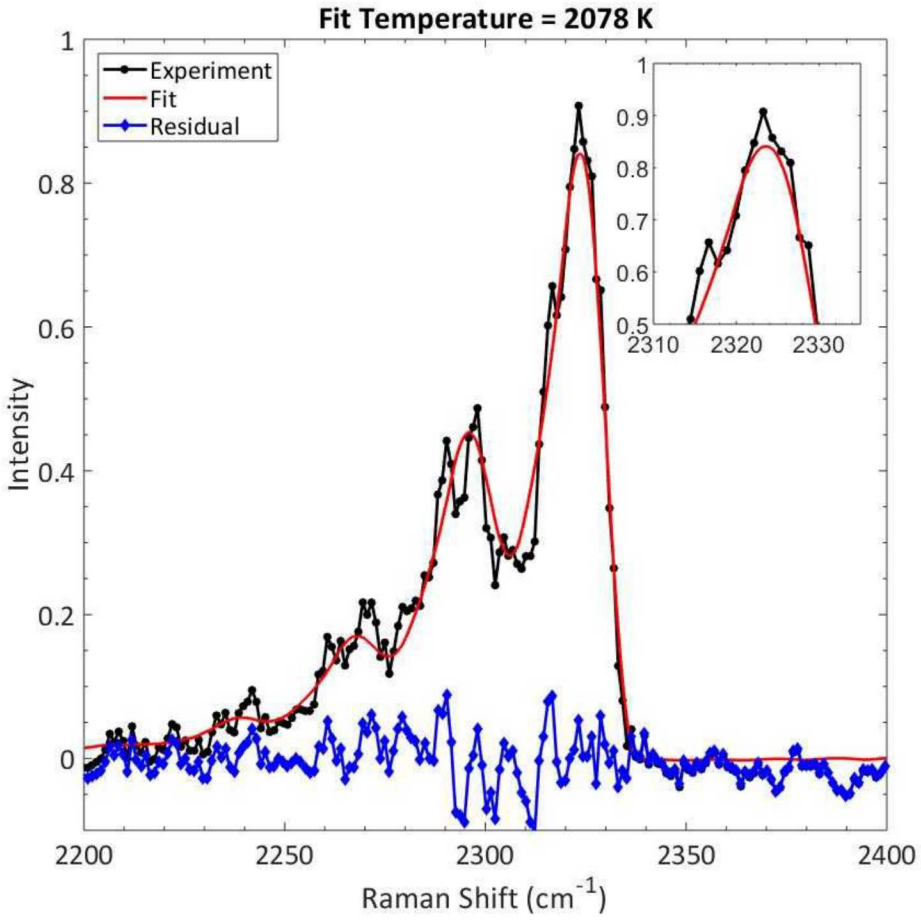

Figure 11: Example 5 kHz Raman spectrum at ϕ = 0.73 with superposed best-fit for temperature.

At higher flame temperatures two factors serve to decrease the SNR: 1) the number density of nitrogen in the atmospheric flame is reduced and 2) the distribution of vibrational population is spread further across multiple states. These effects can be observed by comparing the relative maximum intensities between Fig. 10b and Fig. 11. The inferred temperature from Fig. 11 is T = 2078 K. The mean temperature at this equivalence ratio is 2093 ± 62 K as determined from 31 individual spectra. The decrease in SNR decreases measurement precision, increasing the standard deviation to σ = ± 62 K.

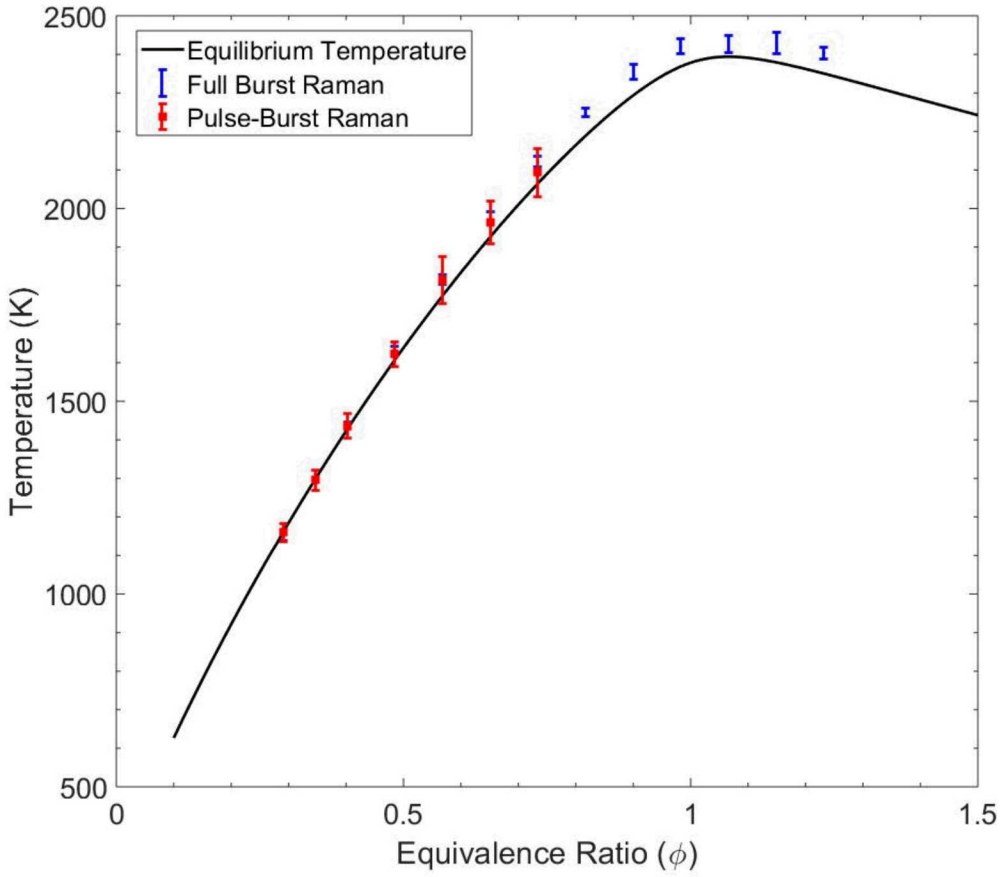

Figure 12: Flame temperature versus equivalence ratios measured by Raman thermometry of the entire burst, with an integration time of 2.5 ms, and Raman thermometry throughout the burst, with an integration time of 200 µs.

For determination of measurement accuracy, Fig. 12 compares the burst-mode thermometry and the full-burst thermometry to calculated chemical equilibrium temperatures. At the leanest H_2-air mixture of $\Phi = 0.29$, the percent difference between pulse-burst and equilibrium temperatures is 0.09%. At the richest equivalence ratio of 0.73, the measurement accuracy decreases to about 3%. Therefore, like the full-burst measurements, the accuracy of the pulse-burst thermometry increases with increased signal to noise.

For each burst, seven frames of Raman spectra were collected. This equates to 1.4 ms of test time in which temperature measurements were acquired every 200 µs. Notably, the present repetition rate of 5 kHz rivals the current state-of-the-art rates of CARS and scanning absorption thermometers [7,10,17]. Naturally, the implementation of a single-laser spontaneous Raman system is far simpler than CARS. Furthermore, in comparison to absorption methods, Raman has the advantage of superior spatial resolution. Pulse-burst Raman spectroscopy therefore offers a robust method for high-speed thermometry that may be amenable to the most challenging measurement environments.

IV. Summary and Future Work

Spectrally resolved Raman thermometry has been assessed in a stabilized flat flame burner to gauge its accuracy and precision as a temperature measurement technique. The burner was run using an H_2-air mixture. Raman spectra were collected from an entire pulse-burst comprised of 25 pulses at 10 kHz burst rate. The laser wavelength was 532 nm and the total burst energy was approximately 13 J. Spectra utilizing the entire 13 J of burst energy served as a baseline over an equivalence ratio range of 0.29 – 1.23. A detailed spectral fitting model determined the adiabatic flame temperature range to be about 1150 K – 2400 K over these equivalence ratios.

Measurements were demonstrated at 5 kHz by integrating two pulses onto a high-speed, back-illuminated EMCCD detector. In the burst-mode measurements, thermometry was performed over an equivalence ratio range of 0.29 – 0.73, corresponding to flame temperatures of 1160 K – 2090 K. The maximum equivalence ratio was limited by SNR considerations. The standard deviation of the 5-kHz Raman thermometry was 2 – 3% of the measured value, dependent on SNR. Here, the burst-mode measurement test time was 1.4 ms, a limit imposed by the number of frames that could be stored on the EMCCD detector. Note that access to longer test times is possible by running the detector in an alternative mode that bins each column of rows prior to final readout. The accuracy of the burst-mode measurement was at worst 3%, indicating that this simple, robust configuration can offer high-speed measurements with high accuracy. This implies that burst-mode Raman spectroscopy may be a useful *in-situ* diagnostic for thermometry in a shock tube or other similar high enthalpy, impulsive systems.

Future work will implement a variant of the present burst-mode Raman thermometry into the Sandia High-Temperature Shock Tube facility. High-speed temperature measurements of dynamic shock-phenomena require considerations of beam delivery, signal collection and signal transfer to the detector. The laser must be passed through sapphire windows with a thickness of 18 mm, which have been measured to reduce the laser incident laser energy by ≤ 16%. Without antireflective coating, an additional loss of Raman signal will occur during collection through another sapphire window. Preliminary optical emission measurements also showed bright, broadband emission from the shock-heated air at high temperatures. This makes SNR considerations critical; polarization filters could be placed in the collection path to remove half of the unpolarized emission. Additionally, the baseline contribution by emission interference could be limited by a set of intensified relay optics (IRO) which would gate the camera exposure time around only the hundreds of nanoseconds where the laser pulse is present in the shock tube.

V. Acknowledgements

This work is supported by the Laboratory Directed Research and Development (LDRD) program at Sandia National Laboratories. The authors would like to thank Tom Grasser for his help with the Hencken burner system. This paper describes objective technical results and analysis. Any subjective views or opinions that might be expressed in the paper do not necessarily represent the views of the U.S. Department of Energy or the United States Government

VI. References

[1] Girard, J. J., & Hanson, R. K. (2017). Minimally intrusive optical probe for in situ shock tube measurements of temperature and species via tunable IR laser absorption. *Applied Physics B*, *123*(11), 264.

[2] Lin, X., Yu, X. L., Li, F., Zhang, S. H., Xin, J. G., & Chang, X. Y. (2013). CO concentration and temperature measurements in a shock tube for Martian mixtures by coupling OES and TDLAS. *Applied Physics B*, *110*(3), 401-409.

[3] Seitzman, J. M., Hanson, R. K., DeBarber, P. A., & Hess, C. F. (1994). Application of quantitative two-line OH planar laser-induced fluorescence for temporally resolved planar thermometry in reacting flows. *Applied Optics*, *33*(18), 4000-4012.

[4] Peuker, J. M., Lynch, P., Krier, H., & Glumac, N. (2013). On AlO emission spectroscopy as a diagnostic in energetic materials testing. *Propellants, Explosives, Pyrotechnics*, *38*(4), 577-585.

[5] Schmidt, J. B., Sands, B., Scofield, J., Gord, J. R., & Roy, S. (2017). Comparison of femtosecond-and nanosecond-two-photon-absorption laser-induced fluorescence (TALIF) of atomic oxygen in atmospheric-pressure plasmas. *Plasma Sources Science and Technology*, *26*(5), 055004.

[6] Frederickson, K., Kearney, S. P., Luketa, A., Hewson, J. C., & Grasser, T. W. (2010). Dual-pump CARS measurements of temperature and oxygen in a turbulent methanol-fueled pool fire. *Combustion Science and Technology*, *182*(8), 941-959.

[7] Kearney, S. P. (2015). Hybrid fs/ps rotational CARS temperature and oxygen measurements in the product gases of canonical flat flames. *Combustion and Flame*, *162*(5), 1748-1758.

[8] Barlow, R. S., Wang, G. H., Anselmo-Filho, P., Sweeney, M. S., & Hochgreb, S. (2009). Application of Raman/Rayleigh/LIF diagnostics in turbulent stratified flames. *Proceedings of the Combustion Institute*, *32*(1), 945-953.

[9] Richardson, D. R., Roy, S., Gord, J. R., & Kearney, S. P. (2017). Two-beam femtosecond rotational CARS for one-dimensional thermometry in a turbulent, sooting jet flame. In *55th AIAA Aerospace Sciences Meeting* (p. 0031).

[10] Roy, S., Hsu, P. S., Jiang, N., Slipchenko, M. N., & Gord, J. R. (2015). 100-kHz-rate gas-phase thermometry using 100-ps pulses from a burst-mode laser. *Optics letters*, *40*(21), 5125-5128.

[11] Magnotti, G., Geyer, D., & Barlow, R. S. (2015). Interference free spontaneous Raman spectroscopy for measurements in rich hydrocarbon flames. *Proceedings of the Combustion Institute*, *35*(3), 3765-3772.

[12] Reising, H. H., Haller, T. W., Clemens, N. T., Varghese, P. L., Fiévet, R., & Raman, V. (2016). Spontaneous Raman Scattering Temperature Measurements and Large Eddy Simulations of Vibrational Non-equilibrium in High-Speed Jet Flames. In *32nd AIAA Aerodynamic Measurement Technology and Ground Testing Conference* (p. 3550).

[13] Utsav, K. C., & Varghese, P. L. (2013). Accurate temperature measurements in flames with high spatial resolution using Stokes Raman scattering from nitrogen in a multiple-pass cell. *Applied optics*, *52*(20), 5007-5021.

[14] Gabet, K. N., Jiang, N., Lempert, W. R., & Sutton, J. A. (2010). Demonstration of high-speed 1D Raman scattering line imaging. *Applied Physics B*, *101*(1-2), 1-5.

[15] Jiang, N., Hsu, P. S., Mance, J. G., Wu, Y., Gragston, M., Zhang, Z., ... & Roy, S. (2017).

High-speed 2D Raman imaging at elevated pressures. *Optics letters*, *42*(18), 3678-3681.

[16] Jiang, N., Roy, S., Hsu, P. S., Mance, J. G., Wu, Y., Gragston, M., ... & Gord, J. R. (2018). High-Speed, Two-dimensional, Multi-species Raman Imaging for Combustion and Flow Diagnostics. In *2018 AIAA Aerospace Sciences Meeting* (p. 2040).

[17] Krishna, Y., Tang, H., Elbaz, A. M., & Magnotti, G. (2019). High-speed Rayleigh–Raman measurements with subframe burst gating. *Optics letters*, *44*(17), 4091-4094.

[18] Eckbreth, A. C. (1996). *Laser diagnostics for combustion temperature and species* (Vol. 3). CRC Press.

[19] Meier, W., Barlow, R. S., Chen, Y. L., & Chen, J. Y. (2000). Raman/Rayleigh/LIF measurements in a turbulent $CH_4/H_2/N_2$ jet diffusion flame: experimental techniques and turbulence–chemistry interaction. *Combustion and Flame*, *123*(3), 326-343.

[20] Kojima, J., & Nguyen, Q. V. (2002). Laser pulse-stretching with multiple optical ring cavities. *Applied optics*, *41*(30), 6360-6370.

[21] Cléon, G., Stepowski, D., & Cessou, A. (2007). Long-cavity Nd: YAG laser used in single-shot spontaneous Raman scattering measurements. *Optics letters*, *32*(22), 3290-3292.

[22] Linstrom, P. J., & Mallard, W. G. (2001). The NIST Chemistry WebBook: A chemical data

resource on the internet. *Journal of Chemical & Engineering Data*, *46*(5), 1059-1063.

[23] Winters, C., & Wagner, J. L. (2019). Interaction of Burst-Mode Laser-Induced-Plasma with an Overexpanded Supersonic Jet at 5–500 kHz Repetition-Rate. In *AIAA Scitech 2019 Forum* (p. 0835).

[24] Goodwin, D.G., Speth, R.L., Moffat, H.K., and Weber, B.W. (2018) Cantera: An object-oriented software toolkit for chemical kinetics, thermodynamics, and transport processes. Version 2.4.0

[25] Hancock, R. D., Bertagnolli, K. E., & Lucht, R. P. (1997). Nitrogen and hydrogen CARS temperature measurements in a hydrogen/air flame using a near-adiabatic flat-flame burner. *Combustion and Flame*, *109*(3), 323-331.